17 Apr 2024

Scanning Electrochemical Microscopy Reveals That Model Silicon Anodes Demonstrate Global Solid Electrolyte Interphase Passivation Degradation During Calendar Aging

Josefine D. McBrayer

Noah B. Schorr

Mila Nhu Lam

Melissa L. Meyerson

et. al. For a complete list of authors, see https://scholarsmine.mst.edu/chem_facwork/3707

Recommended Citation

J. D. McBrayer et al., "Scanning Electrochemical Microscopy Reveals That Model Silicon Anodes Demonstrate Global Solid Electrolyte Interphase Passivation Degradation During Calendar Aging," *ACS Applied Materials and Interfaces*, vol. 16, no. 15, pp. 19663 - 19671, American Chemical Society, Apr 2024. The definitive version is available at https://doi.org/10.1021/acsami.3c14361

ACS APPLIED MATERIALS & INTERFACES

www.acsami.org
Research Article

Scanning Electrochemical Microscopy Reveals That Model Silicon Anodes Demonstrate Global Solid Electrolyte Interphase Passivation Degradation during Calendar Aging

Josefine D. McBrayer,* Noah B. Schorr, Mila Nhu Lam, Melissa L. Meyerson, Katharine L. Harrison,* and Shelley D. Minteer*

Cite This: ACS Appl. Mater. Interfaces 2024, 16, 19663−19671
Read Online

ABSTRACT: Silicon is a promising next-generation anode to increase energy density over commercial graphite anodes, but calendar life remains problematic. In this work, scanning electrochemical microscopy was used to track the site-specific reactivity of a silicon thin film surface over time to determine if undesirable Faradaic reactions were occurring at the formed solid electrolyte interphase (SEI) during calendar aging in four case scenarios: formation between 1.5 V and 100 mV with subsequent rest starting at (1) 1.5 V and (2) 100 mV and formation between 0.75 V and 100 mV with subsequent rest starting at (3) 0.75 V and (4) 100 mV. In all cases, the electrical passivation of silicon decreased with increasing time and potential relative to Li/Li^+ over a 3 day period. Along with the decrease in passivation, the homogeneity of passivation over a 500 μm^2 area decreased with time. Despite some local "hot spots" of reactivity, the areal uniformity of passivation suggests global SEI failure (e.g., SEI dissolution) rather than localized (e.g., cracking) failure. The silicon delithiated to 1.5 V vs Li/Li^+ was less passivated than the lithiated silicon (at the beginning of rest, the forward rate constants, k_f, for ferrocene redox were 7.19×10^{-5} and 3.17×10^{-7} m/s, respectively) and was also found to be more reactive than the pristine silicon surface (k_f of 5×10^{-5} m/s). This reactivity was likely the result of SEI oxidation. When the cell was only delithiated up to 0.75 V versus Li/Li^+, the surface was still passivating (k_f of 6.11×10^{-6} m/s), but still less so than the lithiated surface (k_f of 3.03×10^{-9} m/s). This indicates that the potential of the anode should be kept at or below ~0.75 V vs Li/Li^+ to prevent decreasing SEI passivation. This information will help with tuning the voltage windows for prelithiation in Si half cells and the operating voltage of Si full cells to optimize calendar life. The results provided should encourage the research community to investigate chemical, rather than mechanical, modes of failure during calendar aging and to stop using the typical convention of 1.5 V as a cutoff potential for cycling Si in half cells.

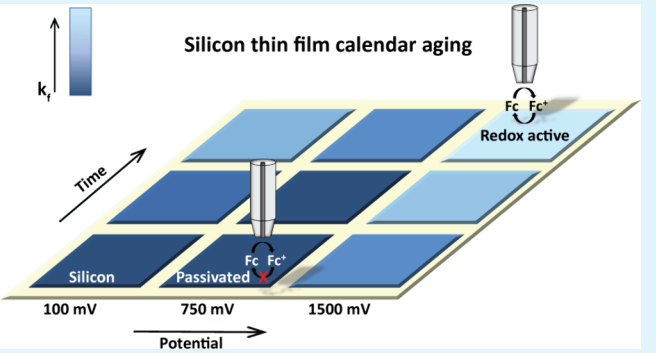

KEYWORDS: *calendar aging, silicon, battery, SECM, passivation, SEI*

INTRODUCTION

Lithium-ion batteries have a broad range of applications, from portable electronics to electric vehicles, and are thus pivotal to society. To further improve performance, new materials must be considered to enhance energy density.[1−4] Silicon is a promising candidate to improve the anode energy density due to a theoretical capacity over 10 times that of graphite and similar operating voltage.[2]

Despite the high capacity of silicon, it suffers from an unstable solid electrolyte interphase (SEI).[5] An effective SEI must be (electro)chemically and mechanically stable, allow for the flow of lithium ions, and block electrons. An effective, passivating SEI is necessary for good cell performance because the continuous reduction of the electrolyte at the anode interface leads to the cell drying out, loss of cyclable lithium, and thickening of the SEI which can hinder lithium-ion diffusion, electronically isolate Si particles, and increase cell resistance.[3,6,7]

The silicon anode SEI is much less passivating than the graphite SEI, and its formation and instability are not as well understood.[7] The over 300% expansion of silicon upon lithiation and delithiation can cause the silicon to crack.[1,8] Reports in the literature suggest this cracking then causes the

Received: September 25, 2023
Revised: February 5, 2024
Accepted: March 18, 2024
Published: April 5, 2024

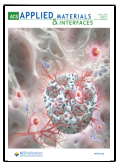

SEI to crack and exposes fresh surfaces for electrolyte reduction.[7,9,10] Despite minimizing silicon cracking through the use of nanomaterials, the SEI remains chemically and mechanically unstable.[1,2,11−14] For example, a breathing behavior has been observed in the silicon SEI where the thickness changes throughout lithiation and delithiation, and SEI stretching has also been observed during cycling, leading to increased porosity and decreased passivation.[15−17] This indicates that the SEI fluctuates greatly and that some of the SEI components are likely soluble in the electrolyte, leading to nonpassivating behavior.

The use of nanomaterials has improved the cycling capability of high-loading silicon anodes, but calendar life, or time-dependent capacity fade of silicon-containing batteries while resting at open circuit, is still far from the goals set forth by the Department of Energy Vehicle Technologies Office.[18] Poor calendar life is the critical remaining barrier that must be overcome to enable the wide adoption of high silicon content anodes in electric vehicles. To improve the calendar life of silicon anodes for lithium-ion batteries, an understanding of the complex mechanical and chemical degradation of the SEI is needed. Degradation mechanisms of the SEI can be classified into two broad groups: mechanical and chemical. Mechanical degradation (e.g., cracking and stretching) will likely require different solutions than chemical degradation (e.g., dissolution, reactivity). The Si cycling research is dominated by developing mitigations for mechanical degradation mechanisms that occur during cycling. Conversely, overcoming calendar aging may require alternative mitigations, because it may be dominated by chemical SEI degradation since cycling and associated volume changes are absent when a cell is at rest. Whether the root cause is mechanical or chemical, the SEI failure mechanisms as a function of potential and time must be better understood. Here, scanning electrochemical microscopy (SECM) is used to collect spatial information on SEI passivation, providing mapping of local (e.g., cracking) versus global SEI passivation (e.g., dissolution, overall poor SEI passivation) failure modes as a function of the state of charge and rest time. To the best of our knowledge, while SECM has been used to study silicon anodes, this is the first direct measurement of Si SEI passivation as a function of calendar aging, to date, in the literature.[14,19]

SECM is an invaluable tool in the investigation of heterogeneous electrode surfaces, making it ideal to understand the open question of whether SEI passivation fails locally due to mechanical mechanisms or globally due to chemical mechanisms during calendar aging. Using a microelectrode probe, the technique is able to quantify local substrate kinetics based on the electrochemical feedback of a redox mediator between the surface and probe.[20] For the Si surface, we chose ferrocene to probe surface reactivity, which has been used in the literature to evaluate SEI passivation.[19,21,22] If the surface is passivated, ferrocene redox peaks are absent in a substrate cyclic voltammogram (CV).[22] However, the redox potential of ferrocene is ∼3.25 V vs Li/Li^+, which is well above potentials where the SEI is expected to be stable,[23,24] so polarizing electrodes through CVs to probe ferrocene activity inherently changes the SEI. SECM removes the possible damage to the SEI that may be caused by polarizing silicon to high potentials. With SECM, the silicon, and therefore the SEI, can be studied at an open circuit or polarized to low potentials where the SEI should be minimally impacted because the SECM probe is polarized to ferrocene potentials instead of the silicon electrode.[14]

This work utilizes the benefits of SECM to track changes in silicon SEI passivation with aging while at rest. Four cases were studied as a function of time at OCV rest: formation between 1.5 V and 100 mV with subsequent rest starting at (1) 1.5 V and (2) 100 mV and formation between 0.75 V and 100 mV with subsequent rest starting at (3) 0.75 V and (4) 100 mV. The silicon delithiated to 1.5 V vs Li/Li^+ was more reactive than the lithiated silicon, whereas when the cell was only delithiated up to 0.75 V versus Li/Li^+, the surface was still passivating. In all cases, the heterogeneity of the surface increased with rest time from the SECM scan taken just after formation to that taken after rest. Despite having local areas of increased reactivity, the overall trends of SEI passivation were predominately global, indicating a chemical degradation route such as SEI dissolution rather than a mechanical mode such as cracking. We expect these findings to guide the research community in focusing on understanding chemical degradation mechanisms during calendar aging and using realistic cutoff potentials in half-cell experiments.

EXPERIMENTAL METHODS

Model silicon thin films were used for all of the experiments. Since both surface kinetics and height changes can affect probe currents, it was confirmed by atomic force microscopy that height changes were less than 100 nm over the radius of the probe (12.5 μm), resulting in minimal impact on the probe current (Figure S1).

Electrode Preparation. Degenerately doped silicon wafers with a low resistivity of 0.004 to 0.04 Ohm-cm were prepared by electron beam evaporation of 50 nm of gold on the backside for improved contact. The front side had three layers, also e-beam evaporated, including 500 nm Cu, 50 nm Si, and 50 nm SiO_2. The samples were diced into 1.75 cm × 1.75 cm squares and then were masked with Kapton tape on half of the front side and the entire backside of the wafer in preparation for alumina deposition. The alumina acted as a pure negative feedback surface for SECM, which allowed for leveling and determination of the exact location of the surface to determine the distance from the sample when doing probe approach curves (PACs) and SECM on the silicon half of the sample (see the Supporting Information in Figure S2 for more information). The Kapton tape allowed the backside and half of the front side to maintain electrical contact once removed following alumina deposition. Alumina was deposited using a Picosun Sunale R150 atomic layer deposition instrument at the Center for Integrated Nanotechnology (CINT). The reactor temperature was either 60 or 200 °C due to changes in equipment capability, but we confirmed that the alumina acted as a pure negative feedback surface at both deposition temperatures. For the 200 °C case, the first precursor was trimethylaluminum (TMA) with a pulse time of 0.1 s and a purge time of 6 s. The carrier gas and flow were N_2 and 150 SCCM, respectively. The TMA temperature was 20 °C. The second precursor was water with a pulse time of 0.1 s and a purge time of 6 s. The carrier gas was also N_2 but with a flow rate of 200 SCCM. Both the TMA and water temperatures were 20 °C. There were 500 cycles resulting in an alumina thickness of ∼ 50 nm. For the 60 °C case, the first precursor was TMA with a pulse time of 0.1 s and a purge time of 15 s. The carrier gas was N_2 flowed at 150 SCCM. The TMA temperature was 20 °C. The second precursor was O_2 at 10−20 SCCM with a pulse time of 26.5 s (includes 2 s valve open flow/pressure stabilization, 24 s plasma on, 0.5 s valve close delay) and a purge time of 10 s. The carrier gas was Ar with a flow rate of 80 SCCM, 2000 W, and temperature of 23 °C.

The Kapton tape was then removed from the silicon side and placed on the alumina side to protect it during further processing steps. The samples were cleaned using O_2 plasma for 3 min. The e-beam evaporated SiO_2 acted as a protective layer to prevent oxidation

https://doi.org/10.1021/acsami.3c14361
ACS Appl. Mater. Interfaces 2024, 16, 19663−19671

of the silicon thin film electrode during these initial processing steps. The SiO_2 layer was then etched using 1% v/v aqueous HF for 4 min to expose the Si surface. The Kapton on the alumina prevented the HF from etching the alumina. The samples were then brought into the glovebox to minimize regrowth of a native oxide.

Electrochemical Measurements. A CH Instruments (CHI) 920D SECM instrument was used for all electrochemical experiments. Pt disk microelectrodes were also purchased from CHI and had a diameter of 25 μm. The probes were polished consecutively using 1 and 0.3 μm alumina paste. The R_g of each electrode is the ratio between the radius of the glass sheath surrounding the Pt wire and the radius of the Pt electrode. The probe tip diameter and approximate R_g were confirmed by optical microscopy and fitting of pure negative feedback PACs (Supporting Information, Figure S2). The PAC of pristine silicon is shown in Figure S3. For all experiments, the silicon substrate was left at open circuit, and the probe was polarized to 3.5 V vs Li/Li^+. The surface kinetics were determined by calculating the rate constant (k_f) using the equations from Lefrou and Cornut.[25]

The cell design is shown in the Supporting Information Figure S4 and has two configurations. The first is for cycling the battery in the electrolyte of interest (40 μL electrolyte volume), and the second is for doing SECM (1 mL electrolyte volume). All electrochemical cycling was performed with gen2 electrolyte from Tomiyama (1.2 M $LiPF_6$ in 3:7 ethylene carbonate: ethylmethyl carbonate). In the cycling configuration, the electrode stack is composed of the substrate (sealed by a Kalrez O-ring), a 2325 Celgard separator, 0.75 mm thick and 8 mm in diameter Li metal, and a Cu rod that makes contact to the lithium. The lithium is gently scraped prior to use. Contact is made to the substrate by pressing indium wire into the back of the conductive substrate and using conductive Cu tape to connect from the indium wire out to an alligator clip. The entire cell body was constructed out of PEEK and the o-rings are Kalrez to prevent reactivity with the silicon substrate and electrolyte.

After cycling and calendar aging tests, the top sealing plate was removed along with the Cu rod, lithium, and separator. Two stainless steel rods were used as contacts to the lithium counter and reference electrodes for the 3-electrode cell configuration. Propylene carbonate (PC) with 100 mM $LiClO_4$ and ~2 mM Fc was added to the side of the electrolyte reservoir to prevent spraying directly on the substrate and disturbing the surface. A discussion on Fc as a redox mediator to probe SEI passivation toward conventional gen2 electrolyte species is in the Supporting Information Figure S5.

Between experiments, the cell bodies were cleaned by rinsing and sonicating sequentially in DI water, acetone, and then IPA for 15 min each (5 min for metal parts). The parts were then dried at 60 °C overnight under dynamic vacuum and hot loaded into the glovebox.

Unless specified otherwise, SECM cells were cycled at 2 $\mu A/cm^2$ in this work. The cells were cycled within an argon glovebox with less than 1 ppm of water and oxygen and were sealed under argon. The case called "delithiated" was cycled 3 times between 100 mV and 1.5 V or 100 mV and 0.75 V and left to rest at open circuit voltage (OCV) in the delithiated state starting at either 1.5 or 0.75 V after a constant voltage hold until the current was less than 0.02 uA/cm^2. The case called "lithiated" was cycled 3 times between 100 mV and 1.5 V or 100 mV and 0.75 V and then lithiated once more to 100 mV and held at a constant voltage until the current was less than 0.02 $\mu A/cm^2$. An example of the 1.5 V case is shown in Figure 1.

The lower voltage cutoff of 100 mV vs Li/Li^+ was selected because several literature sources have reported the actual practical potential at the silicon anode in a full cell to be ~100 mV.[26−29] Using the full range of silicon lithiation provides higher capacity, but it also limits cycle life, so it is common to increase the lower silicon cutoff potential to improve performance. The upper cutoff of 1.5 V vs Li/Li^+ was chosen because this is common in half-cell data in the literature.[24,30−32] The upper cutoff of 0.75 V vs Li/Li^+ was chosen because it is not expected that the silicon voltage in a full cell would go above this value.[33,34] 0.75 V has also been used as a cutoff potential in electrochemical prelithiation of silicon anodes, which is performed in half cells prior to disassembly and full cell fabrication to improve cycle life.[35] Finally, SEI forms below 0.75−0.8 V,[36] so limiting the cutoff potential to 0.75 V keeps the cell in a region where SEI is expected to be stable, rather than being subjected to oxidizing conditions.

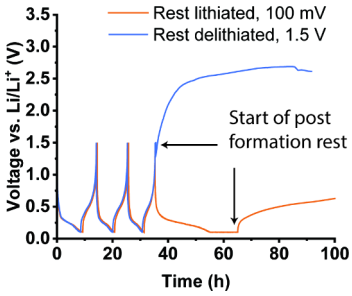

Figure 1. Example of lithiated and delithiated cases with formation cycles between 100 mV and 1.5 V with the constant current of 2 $\mu A/cm^2$ for cycling with a constant voltage at either 100 mV or 1.5 V (held until the current was less than 0.02 $\mu A/cm^2$) prior to entering rest. The cells were left to rest for various amounts of time prior to performing SECM.

The data from the SECM are from multiple cells aging together in tandem, rather than a single cell that was disassembled and investigated at different time points. The reason for this is that the addition of the ferrocene to perform SECM studies contaminated the cell, resulting in anomalous cycling behavior after an SECM measurement was taken. To avoid this, several cells were used, with each cell being used only once per SECM experiment. To ensure consistency, some experiments were repeated to ensure consistent trends of passivation in the lithiated and delithiated states. Since it has been well established in the literature that silicon has poor calendar life,[18,37] this work focuses on understanding SEI passivation changes that could lead to calendar aging rather than on quantifying capacity loss after a rest period.

Characterization. Post-mortem X-ray photoelectron spectroscopy (XPS) measurements were taken on a Kratos AXIS Supra operated at a base pressure better than 2×10^{-9} Torr, using a monochromatic Al Kα X-ray source (λ = 1486.6 eV). Surveys and high-resolution spectra for elements of interest were taken on each sample. Spectra were obtained using a pass energy of 160 eV for all surveys and 20 eV for the high-resolution elements, a step size of 0.1 eV, and a 110 μm aperture.

RESULTS AND DISCUSSION

For both the delithiated and lithiated states in the gen2 electrolyte, the passivation of the SEI decreased with rest time, as shown in Figures 2 and 3. The scale bar shows k_f in m/s for the ferrocene reduction reaction at the Si substrate surface. The larger the value of k_f, the faster the heterogeneous electron transfer and the less passivated the surface is. The large images have the same scale bar to track changes over time. The insets show individually scaled k_f views to show detail for lower k_f values. Figure 2A−C shows the lithiated case when formation was between 100 mV and 1.5 V with increasing rest time from 3 to 26 to 87 h and corresponding average k_f values of 3.2×10^{-7}, 4.7×10^{-7}, and 4.8×10^{-5} m/s, respectively. For A and B, the surface led to negative feedback where the normalized tip current (ratio of the probe current approaching the surface to the steady state current of the probe far from the surface: i/i_{inf}) was less than 1. Negative feedback means the surface is kinetically labile or incapable of reducing Fc^+ generated at the tip, preventing Fc reoxidation by the tip and shutting down the redox loop between the substrate and tip. Positive feedback occurs when the surface is kinetically facile and capable of reducing Fc^+ generated at the tip that then gets reoxidized at the tip creating a feedback loop. At 87 h, the previously

https://doi.org/10.1021/acsami.3c14361
ACS Appl. Mater. Interfaces 2024, 16, 19663−19671

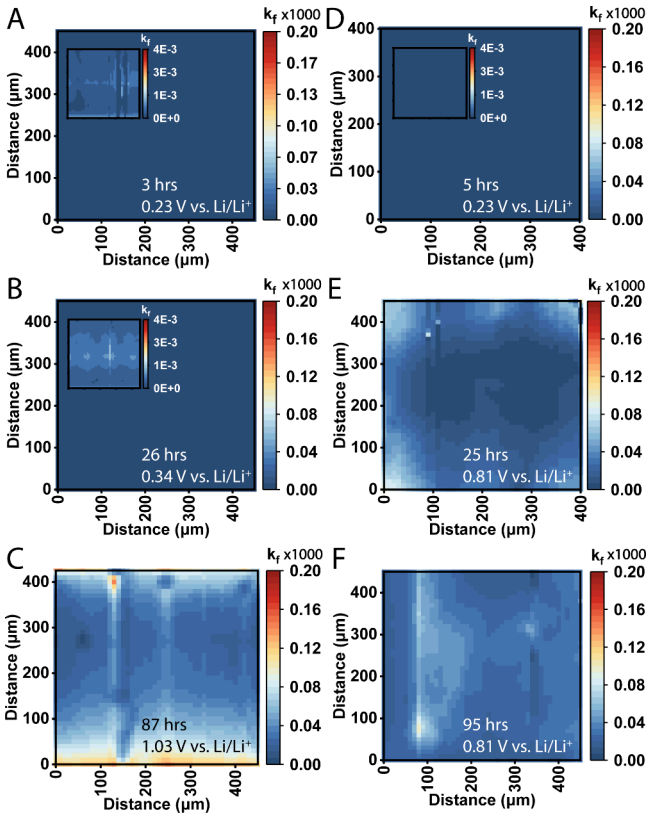

Figure 2. SECM images of the silicon thin films that have undergone three formation cycles between 100 mVand 1.5 V (A−C) and 100 mV and 0.75 V (D−F) and then left to rest in the lithiated state for the indicated times starting at 100 mV. The rest time and measured voltage at the start of the SECM experiment are shown in the bottom right of each image. All images show k_f (m/s) on the same scale with the insets showing individually scaled images. The 12.5 μm radius probe was polarized to 3.5 V vs Li/Li$^+$ and the substrate was unpolarized.

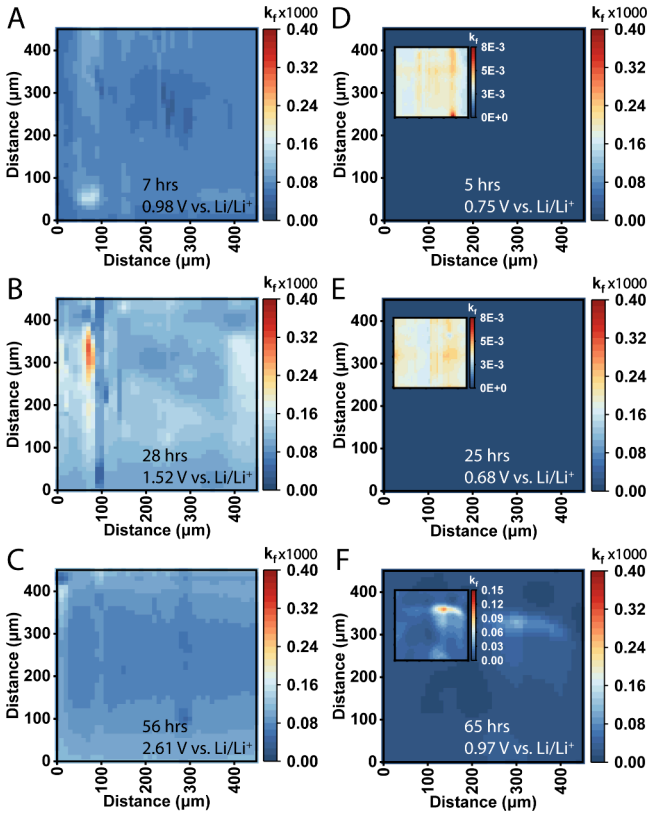

Figure 3. SECM images of the silicon thin films that have undergone three formation cycles between 100 mV and 1.5 V (A−C) and 100 mV and 0.75 V (D−F) and then left to rest in the delithiated state for the indicated times starting at 1.5 V (A−C) and 0.75 V (D−F). The rest time and measured voltage at the start of the SECM experiment are shown in the bottom right of each image. All images show k_f (m/s) on the same scale with the insets showing individually scaled images. The 12.5 μm radius probe was polarized to 3.5 V vs Li/Li$^+$, and the substrate was unpolarized.

lithiated surface (which at 87 h transitioned to fully delithiated) started to exhibit positive feedback behavior with a normalized tip current greater than 1, indicating an increase in surface electron transfer reactivity. These trends were confirmed by doing substrate CVs at the end of an experiment as seen by the absence or appearance of Fc redox peaks (Supporting Information Figure S6). Figure 2D−F shows the lithiated case for formation between 100 mV and 0.75 V, the motivation for which will be discussed subsequently. A similar increase in reactivity is observed over time but changes more rapidly initially, followed by a more passivated surface after 95 h.

The surface of the silicon delithiated to 1.5 V (Figure 3A−C) was more reactive than the lithiated surface (Figure 2A−C) at all times, as evident from the average k_f values shown in Figure 4A where all conditions are compared on the same scale. For the 1.5 V delithiated state (Figure 3A−C), the data were collected at 7, 28, and 56 h with corresponding average k_f values of 7.2×10^{-5}, 1.2×10^{-4}, and 8.5×10^{-5} m/s, respectively. The k_f values at short rest times are an order of magnitude smaller in the lithiated case (Figure 2A−C) in comparison to the delithiated to 1.5 V case (Figure 3A−C). In the main text, Figures 2 and 3 are scaled individually to see differences more easily as a function of time and potential. Figure 2 is shown in the Supporting Information (Figure S7) on the same scale as Figure 3 for comparison between the delithiated and lithiated cases. For all times, the delithiated surface exhibited enhanced feedback where the normalized tip current was greater than 1. This would imply that the calendar aging of silicon-containing batteries would be worse in the discharged state than the charged state of a full cell, but it is commonly accepted that lithium-ion batteries age faster in the charged state. The top voltage cutoff for the SECM half cells was chosen because half cells are commonly cycled between 50 or 100 mV and 1.5 V in the literature.[3,5,6] However, silicon anodes in full cells would realistically not go beyond about 0.6−0.75 V. To investigate if the high potential of 1.5 V was causing damage to the SEI that might lead to this unexpected result, the delithiation experiment was repeated with formation cycles performed between 0.75 and 100 mV, ending with delithiation to 0.75 V (Figure 3D−F). The upper voltage cutoff of 0.75 V was chosen because it has been used as the cutoff for half-cell prelithiation cycling,[35] has been shown to be the maximum silicon voltage in a full cell,[33,34] and keeps the SEI below SEI formation potentials to protect it against potential electrochemical oxidation.[36]

The surface delithiated to 0.75 V was much more passivated than when delithiated to 1.5 V, proving that the SEI becomes nonpassivating at too high of a potential. The aging of the 0.75 V delithiated case is similar to aging in the lithiated case, as

https://doi.org/10.1021/acsami.3c14361
ACS Appl. Mater. Interfaces 2024, 16, 19663−19671

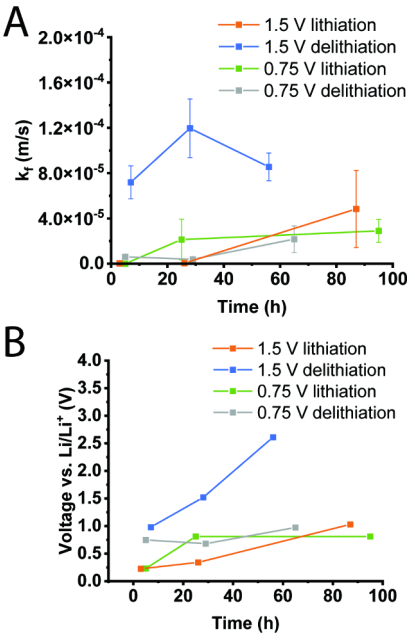

Figure 4. (A) Average k_f values corresponding to the images shown in Figures 2 and 3. The error bars are the standard deviation of the average within a given image to quantify the heterogeneity of the surface within one image rather than the error bars providing a measure of image to image variation for the same condition. (B) Voltage measured at the start of the SECM experiment after rest.

seen in Figure 4, in that both exhibit negative feedback (unlike the 1.5 V case). Accelerated aging in the charged state relative to the discharged state in full cells is also affected by the cathode, which is not observed in half-cell experiments. Recent silicon literature indicates that the impedance rise during calendar aging in the charged state came predominately from the cathode. Despite the loss of lithium resulting in loss of capacity, changes in the impedance of the anode were small.[27] This implies that although there was capacity loss due to continuous SEI formation, the SEI was not becoming thicker or more resistive and increasing impedance. Therefore, this work suggests that our results showing similar passivation in the "charged" and "discharged" states (0.1 and 0.75 V) are not as surprising as they may first seem because the significant changes between the charged and discharged state that one intuitively expects are taking place at the cathode rather than the anode. Furthermore, the higher reactivity at 1.5 V vs Li/Li^+ is supported by the literature as well.[16,23] Hasa et al.[23] observed the dissolution of LiEDC at 1.5 V, which may contribute to the poor passivation at this higher potential. Zhuo et al.[16] showed that the SEI can be reversibly cycled to capacities that increase with potential, indicating that SEI species can be oxidized and reduced electrochemically. Degradation of the SEI has implications for half-cell electrochemical prelithiation as well as proof of performance cycling in half cells for new electrolytes, electrode materials, and architectures. An SEI that degrades during delithiation to 1.5 V would not necessarily manifest as capacity fade in typical half cells with excess lithium inventory because there is enough lithium to rebuild the SEI each cycle, and it may also lead to erroneously low Coulombic efficiency measurements at the working electrode when evaluating new materials. The continual degradation/formation of the SEI in a half cell could lead to a structure different from what would form under full cell conditions. This would also affect electrochemical prelithiation of silicon anodes because delithiating to too high of a potential may be detrimental to the SEI and negate the purpose of prelithiating to overcome initial irreversible losses due to SEI formation and lithiation of high-impedance sites within the silicon anode. Degradation of the SEI in these SECM experiments just means that it has lost its ability to passivate the surface, but it does not necessarily mean that the SEI has been completely removed.

To help better visualize the change in the surface over time, the images in Figures 2 and 3 were averaged and plotted as a function of the rest time (Figure 4). Passivation generally stays approximately the same or decreases with rest time, with the exception of the 1.5 V delithiated case, which showed greater reactivity at 28 h than 56 h. This may be due to cell-to-cell variability or behavior starting to plateau as a function of time. The lithiated surface remains more passivated than the initial Si surface until 87 h where the surface became more reactive than the initial surface (average k_f of 5×10^{-5} m/s as shown in Figure S8). The potential rose to 1.03 V at 87 h and is fully delithiated. At the beginning of rest, the 1.5 V surface is already as reactive as the original silicon surface without any SEI present and then becomes more reactive with increasing time. The delithiated surface rested at 0.75 V, however, remains comparable to the lithiated surface passivation. These average tabulations reiterate that delithiation to 1.5 V leads to SEI and passivation degradation. The concept of needing to check the voltage range of SEI oxidation stability for a specific anode active material and electrolyte is important for the research community to consider. The SEI on copper has been shown to decompose during the oxidation process as well.[16] SECM can be a useful tool to determine the optimal operating conditions for SEI formed with different cell chemistries.

The error bars in Figure 4 are the standard deviation of the average k_f within a given image taken over 500 μm^2 areas and can be used to understand passivation homogeneity, which has implications for determining mechanisms of passivation failure. In both the lithiated and delithiated cases, the heterogeneity of passivation increases from the initial surface with minimal rest. The first data point at around 5−10 h is highly homogeneous, whereas all the higher rest times have increased heterogeneity, although this does not increase linearly with time. While there are often more "hot spots" (larger error bars in average k_f) in SEI passivation after rest than immediately after formation, the electron transfer rate was reasonably comparable across the surface in each sample. The increase in passivation heterogeneity does not manifest as distinct SEI cracks (see images in Figures 2 and 3), but rather broad areas of faster kinetics. The change in passivation with the change in potential may be correlated to the "breathing" mechanism of the silicon SEI,[15,24] where the SEI becomes thicker as the silicon is delithiated and thinner during lithiation. Additionally, the SEI structure or porosity may change with time at rest or with the state of charge. Stetson et al. observed a decrease in SEI resistivity with rest which they hypothesized was the dissolution of the outer organic layer of the SEI, exposing the more inorganic inner layer of the SEI.[38] Their result is consistent with the work reported here, with both sets of results indicating that the SEI does not equilibrate over the test duration. Yoon et al. observed that volume change of Si anodes introduces porosity into the SEI layer, which can lead to reactivity with electrolyte components.[17] The rapid, as compared to a composite electrode, change in potential during

https://doi.org/10.1021/acsami.3c14361
ACS Appl. Mater. Interfaces 2024, 16, 19663−19671

rest of the thin films means fairly rapid delithiation and therefore volume change, which likely further disturbs the SEI during OCV aging. One or several of these mechanisms may be contributing to increased heterogeneity.

To understand how the SEI is chemically changing with rest, the samples cycled between 100 and 0.75 V were analyzed with XPS as shown in the Supporting Information Figure S9. Aging at rest results in a drastic change in the chemical composition of the surface. The fraction of the signal for SEI components containing C, F, and O decreases with rest, suggesting there is less SEI on the surface. The decrease in F compounds (such as LiF), lithium carbonate, and organic compounds (containing sp^3 and sp^2 carbon bonds) with time suggests that both the inorganic and organic species are being consumed or are dissolving. Evidence of lithiation (for example, Li_4SiO_4) also goes away with rest indicating self-discharge in agreement with the observed increasing voltage in the cell during rest. The species that remain tend to become more varied, supporting the SECM observation of increasing SEI heterogeneity with rest relative to that after formation.

When the Si anode is aged at OCV, there are two variables that can affect the passivation of the electrodes. The first is time, which can lead to degradation of the SEI by a variety of mechanisms; for example, dissolution/thickening or cracking of the SEI as the electrode loses lithium. The second variable is the change in potential as the electrode loses lithium, which can also change the character of the SEI. Figure 4 shows the average k_f and cell potential as functions of rest time. The driving factor for changes in passivation is unclear because of the rapid change in potential inherent to silicon thin films (rather than silicon composite electrodes). This phenomena with thin films could be related to a variety of mechanisms. An example is that SEI dissolution may be related to solubility limits within the size of local pore volumes in a porous electrode and the accessible volumes next to the surface may be significantly different in a thin film. This would lead to different SEI dissolution rates in a thin film versus porous electrode. To determine which variable impacts passivation more, an experiment was conducted where the same 3 formation cycles were performed, but rather than resting after lithiation, the cell was galvanostatically charged and held at the potential the cell reached after ~3 days of rest (810 mV). Immediately after the current relaxed to 0.02 $\mu A/cm^2$ during the voltage hold at 810 mV, SECM was performed. As seen in Figure 5, the passivation is much higher in the case without rest as opposed to the case with rest, where the potential rose naturally to 810 mV, despite the latter being held at the same potential. This indicates that increasing rest time, rather than the potential, is the major driving force for the decrease in SEI passivation in the potential regime up to around 800 mV, though these SECM data also show that driving the potential too high (1.5 V) when delithiating can also induce damage to the SEI. This is an important result for providing validity for making comparisons of the different cells over time since the nature of the experiment made comparisons at the exact same time difficult. Because time is the main driver of passivation, comparing overall trends with time (Figure 4) between samples is reliable. This result also suggests that the loss of SEI passivation is chemically rather than electrochemically driven when the potential is relatively low (<810 mV). Although the exact mechanism cannot be deciphered from these SECM experiments, dissolution of SEI components into the electrolyte is consistent with the SECM and XPS results.

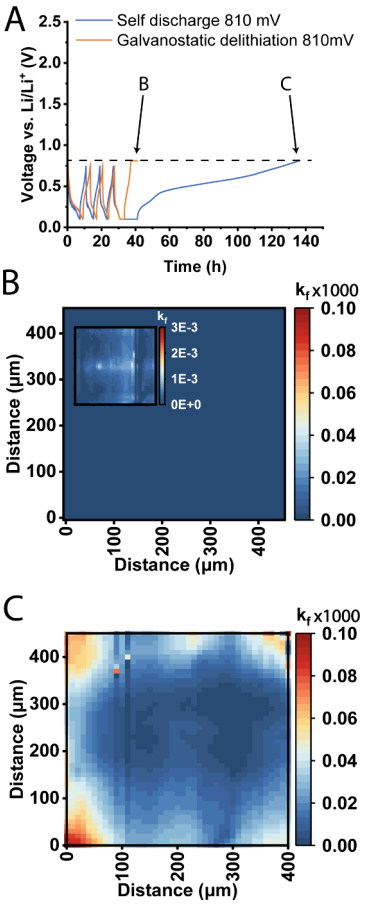

Figure 5. (A) Experiment protocol used to check if passivation is primarily dictated by voltage or the amount of rest time. In the self-discharge case, the cell was cycled three times between 100 mV and 0.75 V and then held at a constant voltage at 100 mV until the current was less than 0.02 $\mu A/cm^2$ and then left to rest for 95 h before SECM was performed. The cell was at 810 mV when the SECM experiment began. In the galvanostatic delithiation case, the cell was cycled three times between 100 mV and 0.75 V, held at a constant voltage at 100 mV until the current was less than 0.02 $\mu A/cm^2$, and then was galvanostatically delithiated to 810 mV and held there until the current was less than 0.02 $\mu A/cm^2$. (B) SECM image of the galvanostatic delithiation case. (C) SECM image of the self-discharge case. The (B) and (C) with arrows in (A) correspond to the time when the SECM images in (B) and (C) were collected.

CONCLUSIONS

Calendar aging of silicon anodes for lithium-ion batteries is a limiting factor for widespread commercialization of high silicon loading cells. A better understanding of SEI failure during rest is needed in order to limit capacity fade with calendar aging. Here, for the first time, SECM imaging of Si nanofilms showed the surface passivation generally decreases with increasing open circuit rest time and corresponding increasing potential relative to Li/Li^+ (as the material self-discharges). However, the time of rest, rather than the potential change during rest, was found to ultimately determine the level of passivation of the silicon thin film at relatively low potentials below 810 mV. Although the exact degradation mechanism during calendar aging cannot be determined from this work alone, this research does help eliminate possible degradation routes. As passivation

https://doi.org/10.1021/acsami.3c14361
ACS Appl. Mater. Interfaces 2024, 16, 19663−19671

decreases over time, the homogeneity of passivation also decreases. Despite some local "hot spots" of reactivity, within resolution limits (tip radius of 12.5 μm), the changes in passivation seemed to be global SEI degradation (for example, SEI dissolution) rather than local (for example, cracking). This suggests that SEI degradation during calendar aging of silicon anodes is related to global chemical or small scale (less than 12.5 μm) mechanical instability mechanisms rather than macroscale mechanical instability mechanisms. This was supported by XPS which suggested the dissolution of the SEI with rest.

At all times aged, the silicon delithiated to 1.5 V vs Li/Li^+ was more reactive than the lithiated silicon. When the cell was delithiated only up to 0.75 V versus Li/Li^+, the surface was still passivating. This indicates that the potential of the anode should be kept at or below ~0.75 V for half cell, full cell, and electrochemical prelithiation cycling to prevent decreasing SEI passivation. This is important to understand because the battery community regularly employs a 1.5 V cutoff potential in half-cell tests, which may be leading to SEI degradation that would not be present in full cells.

Based on this work, we urge the research community to focus on exploring chemical routes of calendar aging rather than the typical focus on the mechanical issues with silicon. Future research directions that could be helpful in improving silicon calendar life include (1) voltage profile optimization of both prelithiation and full cells, (2) exploration of different electrolytes to see if passivation over time improves, (3) surface treatments of silicon aimed at improving the SEI stability with time, and (4) further SECM experiments using more relevant counter electrodes such as lithium iron phosphate or lithium nickel manganese cobalt oxide cathodes to see the effect, if any, on silicon passivation over time.

■ ASSOCIATED CONTENT

Supporting Information

The Supporting Information is available free of charge at https://pubs.acs.org/doi/10.1021/acsami.3c14361.

Atomic force microscope image of pristine silicon surface; probe approach curve of alumina pure negative feedback; probe approach curve of silicon before and after cycling; cell design; cyclic voltammogram of Pt microelectrode; cyclic voltammogram of macrosilicon electrode over time; SECM image of pristine silicon surface; and XPS spectra of 100 and 750 mV before and after rest (PDF)

■ AUTHOR INFORMATION

Corresponding Authors

Josefine D. McBrayer − *Power Sources Technology Group, Sandia National Laboratory, Albuquerque, New Mexico 5800, United States;* orcid.org/0000-0002-2252-5786; Email: jdmcbra@sandia.gov

Katharine L. Harrison − *Materials Science Center, National Renewable Energy Laboratory, Golden, Colorado 80401, United States;* orcid.org/0000-0002-5807-6919; Email: katie.harrison@nrel.gov

Shelley D. Minteer − *Department of Chemistry, University of Utah, Salt Lake City, Utah 84112, United States; Kummer Institute Center for Resource Sustainability, Missouri University of Science and Technology, Rolla, Missouri 65409, United States;* orcid.org/0000-0002-5788-2249; Email: minteer@chem.utah.edu

Authors

Noah B. Schorr − *Power Sources Technology Group, Sandia National Laboratory, Albuquerque, New Mexico 5800, United States;* orcid.org/0000-0002-1582-8594

Mila Nhu Lam − *Materials Characterization and Performance Department, Sandia National Laboratory, Albuquerque, New Mexico 5800, United States;* orcid.org/0000-0001-5161-6604

Melissa L. Meyerson − *Materials Characterization and Performance Department, Sandia National Laboratory, Albuquerque, New Mexico 5800, United States;* orcid.org/0000-0001-9327-442X

Complete contact information is available at: https://pubs.acs.org/10.1021/acsami.3c14361

Notes

The authors declare no competing financial interest.

■ ACKNOWLEDGMENTS

This work was performed, in part, at the Center for Integrated Nanotechnologies, an Office of Science User Facility operated for the U.S. Department of Energy (DOE) Office of Science. Sandia National Laboratories is a multimission laboratory managed and operated by the National Technology and Engineering Solutions of Sandia, LLC (NTESS), a wholly owned subsidiary of Honeywell International Inc., for the U.S. Department of Energy's National Nuclear Security Administration (DOE/NNSA) under contract DE-NA0003525. This written work is authored by an employee of NTESS. The employee, not NTESS, owns the right, title and interest in and to the written work and is responsible for its contents. Any subjective views or opinions that might be expressed in the written work do not necessarily represent the views of the U.S. Government. The publisher acknowledges that the U.S. Government retains a nonexclusive, paid-up, irrevocable, worldwide license to publish or reproduce the published form of this written work or allow others to do so, for U.S. Government purposes. The DOE will provide public access to results of federally sponsored research in accordance with the DOE Public Access Plan. This research was supported by the U.S. Department of Energy's Vehicle Technologies Office under the Silicon Consortium Project, directed by Brian Cunningham, and managed by Anthony Burrell. This work was authored in part by the National Renewable Energy Laboratory, operated by Alliance for Sustainable Energy, LLC, for the U.S. Department of Energy (DOE) under Contract No. DE-AC36-08GO28308. The views expressed in the article do not necessarily represent the views of the DOE or the U.S. Government. The U.S. Government retains and the publisher, by accepting the article for publication, acknowledges that the U.S. Government retains a nonexclusive, paid-up, irrevocable, worldwide license to publish or reproduce the published form of this work, or allow others to do so, for U.S. Government purposes. The authors of this work would like to acknowledge John Paul Bullivant for ALD deposition, Benjamin Warren for ALD deposition, and Cooper Bryan for cleaning cell components.

REFERENCES

(1) Gonzalez, A. F.; Yang, N. H.; Liu, R. S. Silicon Anode Design for Lithium-Ion Batteries: Progress and Perspectives. *J. Phys. Chem. C* **2017**, *121* (50), 27775−27787.

(2) Ryu, J.; Hong, D.; Lee, H. W.; Park, S. Practical considerations of Si-based anodes for lithium-ion battery applications. *Nano Res.* **2017**, *10* (12), 3970−4002.

(3) Luo, W.; Chen, X. Q.; Xia, Y.; Chen, M.; Wang, L. J.; Wang, Q. Q.; Li, W.; Yang, J. P. Surface and Interface Engineering of Silicon-Based Anode Materials for Lithium-Ion Batteries. *Adv. Energy Mater.* **2017**, *7* (24), No. 1701083, DOI: 10.1002/aenm.201701083.

(4) McDowell, M. T.; Lee, S. W.; Nix, W. D.; Cui, Y. 25th Anniversary Article: Understanding the Lithiation of Silicon and Other Alloying Anodes for Lithium-Ion Batteries. *Adv. Mater.* **2013**, *25* (36), 4966−4984.

(5) Yin, Y.; Arca, E.; Wang, L.; Yang, G.; Schnabel, M.; Cao, L.; Xiao, C.; Zhou, H.; Liu, P.; Nanda, J.; Teeter, G.; Eichhorn, B.; Xu, K.; Burrell, A.; Ban, C. Nonpassivated Silicon Anode Surface. *Acs Appl. Mater. Inter* **2020**, *12* (23), 26593−26600.

(6) Sun, F.; Markotter, H.; Dong, K.; Manke, I.; Hilger, A.; Kardjilov, N.; Banhart, J. Investigation of failure mechanisms in silicon based half cells during the first cycle by micro X-ray tomography and radiography. *J. Power Sources* **2016**, *321*, 174−184.

(7) Wang, Y. K.; Zhang, Q. L.; Li, D. W.; Hu, J. Z.; Xu, J. G.; Dang, D. Y.; Xiao, X. C.; Cheng, Y. T. Mechanical Property Evolution of Silicon Composite Electrodes Studied by Environmental Nano-indentation. *Adv. Energy Mater.* **2018**, *8* (10), No. 1702578, DOI: 10.1002/aenm.201702578.

(8) Gu, M.; Wang, Z. G.; Connell, J. G.; Perea, D. E.; Lauhon, L. J.; Gao, F.; Wang, C. M. Electronic Origin for the Phase Transition from Amorphous LixSi to Crystalline Li15Si4. *ACS Nano* **2013**, *7* (7), 6303−6309.

(9) Haruta, M.; Kijima, Y.; Hioki, R.; Doi, T.; Inaba, M. Artificial lithium fluoride surface coating on silicon negative electrodes for the inhibition of electrolyte decomposition in lithium-ion batteries: visualization of a solid electrolyte interphase using in situ AFM. *Nanoscale* **2018**, *10* (36), 17257−17264.

(10) Kumar, R.; Lu, P.; Xiao, X. C.; Huang, Z. Q.; Sheldon, B. W. Strain-Induced Lithium Losses in the Solid Electrolyte Interphase on Silicon Electrodes. *Acs Appl. Mater. Inter* **2017**, *9* (34), 28406−28417.

(11) Son, Y.; Jaekyung, S.; Son, Y.; Cho, J. Recent progress of analysis techniques for silicon-based anode of lithium-ion batteries. *Curr. Opin. Electrochem.* **2017**, *6*, 77−83.

(12) Liu, X. H.; Zhong, L.; Huang, S.; Mao, S. X.; Zhu, T.; Huang, J. Y. Size-Dependent Fracture of Silicon Nanoparticles During Lithiation. *ACS Nano* **2012**, *6* (2), 1522−1531.

(13) Gao, Y.; Yi, R.; Li, Y. C. G.; Song, J. X.; Chen, S. R.; Huang, Q. Q.; Mallouk, T. E.; Wang, D. H. General Method of Manipulating Formation, Composition, and Morphology of Solid-Electrolyte Interphases for Stable Li-Alloy Anodes. *J. Am. Chem. Soc.* **2017**, *139* (48), 17359−17367.

(14) Ventosa, E.; Wilde, P.; Zinn, A. H.; Trautmann, M.; Ludwig, A.; Schuhmann, W. Understanding surface reactivity of Si electrodes in Li-ion batteries by in operando scanning electrochemical microscopy. *Chem. Commun.* **2016**, *52* (41), 6825−6828.

(15) Veith, G. M.; Doucet, M.; Baldwin, J. K.; Sacci, R. L.; Fears, T. M.; Wang, Y. Q.; Browning, J. F. Direct Determination of Solid-Electrolyte Interphase Thickness and Composition as a Function of State of Charge on a Silicon Anode. *J. Phys. Chem. C* **2015**, *119* (35), 20339−20349.

(16) Zhuo, Z. Q.; Lu, P.; Delacourt, C.; Qiao, R. M.; Xu, K.; Pan, F.; Harris, S. J.; Yang, W. L. Breathing and oscillating growth of solid-electrolyte-interphase upon electrochemical cycling. *Chem. Commun.* **2018**, *54* (7), 814−817.

(17) Yoon, I.; Larson, J. M.; Kostecki, R. The Effect of the SEI Layer Mechanical Deformation on the Passivity of a Si Anode in Organic Carbonate Electrolytes. *ACS Nano* **2023**, *17* (7), 6943−6954.

(18) McBrayer, J. D.; Rodrigues, M.-T. F.; Schulze, M. C.; Abraham, D. P.; Apblett, C. A.; Bloom, I.; Carroll, G. M.; Colclasure, A. M.; Fang, C.; Harrison, K. L.; Liu, G.; Minteer, S. D.; Neale, N. R.; Veith, G. M.; Johnson, C. S.; Vaughey, J. T.; Burrell, A. K.; Cunningham, B. Calendar aging of silicon-containing batteries. *Nature Energy* **2021**, *6* (9), 866−872.

(19) Jiyane, N.; García-Quismondo, E.; Ventosa, E.; Schuhmann, W.; Santos, C. S. Elucidating Degradation Mechanisms of Silicon-graphite Electrodes in Lithium-ion Batteries by Local Electrochemistry. *Batteries Supercaps* **2023**, *6* (8), No. e202300126.

(20) Polcari, D.; Dauphin-Ducharme, P.; Mauzeroll, J. Scanning Electrochemical Microscopy: A Comprehensive Review of Experimental Parameters from 1989 to 2015. *Chem. Rev.* **2016**, *116* (22), 13234−13278.

(21) Tang, M.; Newman, J. Electrochemical Characterization of SEI-Type Passivating Films Using Redox Shuttles. *J. Electrochem. Soc.* **2011**, *158* (5), A530.

(22) Dinh-Nguyen, M. T.; Delacourt, C. Investigation of the Passivation Properties of the Solid Electrolyte Interphase Using a Soluble Redox Couple. *J. Electrochem. Soc.* **2016**, *163* (5), A706.

(23) Hasa, I. A.-O.; Haregewoin, A. A.-O.; Zhang, L. A.-O.; Tsai, W. Y.; Guo, J. A.-O.; Veith, G. A.-O.; Ross, P. N.; Kostecki, R. Electrochemical Reactivity and Passivation of Silicon Thin-Film Electrodes in Organic Carbonate Electrolytes. *ACS Appl. Mater. Interfaces* **2020**, *12*, 40879−40890, DOI: 10.1021/acsami.0c09384.

(24) Veith, G. M.; Doucet, M.; Sacci, R. L.; Vacaliuc, B.; Baldwin, J. K.; Browning, J. F. Determination of the Solid Electrolyte Interphase Structure Grown on a Silicon Electrode Using a Fluoroethylene Carbonate Additive. *Sci. Rep.* **2017**, *7*, 6326.

(25) Lefrou, C.; Cornut, R. Analytical expressions for quantitative scanning electrochemical microscopy (SECM). *ChemPhysChem* **2010**, *11*, 547−556, DOI: 10.1002/cphc.200900600.

(26) Rodrigues, M.-T. F.; Prado, A. Y. R.; Trask, S. E.; Ahmed, S.; Jansen, A. N.; Abraham, D. P. Modulating electrode utilization in lithium-ion cells with silicon-bearing anodes. *J. Power Sources* **2020**, *477*, No. 229029.

(27) F. Rodrigues, M.-T.; Yang, Z.; Trask, S. E.; Dunlop, A. R.; Kim, M.; Dogan, F.; Key, B.; Bloom, I.; Abraham, D. P.; Jansen, A. N. Pouch cells with 15% silicon calendar-aged for 4 years. *J. Power Sources* **2023**, *565*, No. 232894.

(28) Leveau, L.; Laïk, B.; Pereira-Ramos, J.-P.; Gohier, A.; Tran-Van, P.; Cojocaru, C.-S. Cycling strategies for optimizing silicon nanowires performance as negative electrode for lithium battery. *Electrochim. Acta* **2015**, *157*, 218−224.

(29) Arnot, D. J.; Allcorn, E.; Harrison, K. L. Effect of Temperature and FEC on Silicon Anode Heat Generation Measured by Isothermal Microcalorimetry. *J. Electrochem. Soc.* **2021**, *168* (11), No. 110509.

(30) Schulze, M. C.; Neale, N. R. Half-Cell Cumulative Efficiency Forecasts Full-Cell Capacity Retention in Lithium-Ion Batteries. *ACS Energy Letters* **2021**, *6* (3), 1082−1086.

(31) Yang, G.; Frisco, S.; Tao, R.; Philip, N.; Bennett, T. H.; Stetson, C.; Zhang, J.-G.; Han, S.-D.; Teeter, G.; Harvey, S. P.; Zhang, Y.; Veith, G. M.; Nanda, J. Robust Solid/Electrolyte Interphase (SEI) Formation on Si Anodes Using Glyme-Based Electrolytes. *ACS Energy Letters* **2021**, *6* (5), 1684−1693.

(32) Jia, H.; Li, X.; Song, J.; Zhang, X.; Luo, L.; He, Y.; Li, B.; Cai, Y.; Hu, S.; Xiao, X.; Wang, C.; Rosso, K. M.; Yi, R.; Patel, R.; Zhang, J.-G. Hierarchical porous silicon structures with extraordinary mechanical strength as high-performance lithium-ion battery anodes. *Nat. Commun.* **2020**, *11* (1), 1474.

(33) Luo, M.; F. Rodrigues, M.-T.; Shaw, L. L.; Abraham, D. P. Examining Effects of Negative to Positive Capacity Ratio in Three-Electrode Lithium-Ion Cells with Layered Oxide Cathode and Si Anode. *ACS Appl. Energy Mater.* **2022**, *5* (5), 5513−5518.

(34) Rodrigues, M.-T. F.; Gilbert, J. A.; Kalaga, K.; Abraham, D. P. Insights on the cycling behavior of a highly-prelithiated silicon−graphite electrode in lithium-ion cells. *Journal of Physics: Energy* **2020**, *2* (2), No. 024002.

(35) Schulze, M. C.; Fink, K.; Palmer, J.; Carroll, G. M.; Dutta, N. S.; Zwiefel, C.; Engtrakul, C.; Han, S.-D.; Neale, N. R.; Tremolet de Villers, B. J. Pitch Carbon-coated Ultrasmall Si Nanoparticle Lithium-

ion Battery Anodes Exhibiting Reduced Reactivity with Carbonate-based Electrolyte. *Batteries Supercaps* **2023**, *6* (9), No. e202300186.
(36) Wu, Z.-Y.; Lu, Y.-Q.; Li, J.-T.; Zanna, S.; Seyeux, A.; Huang, L.; Sun, S.-G.; Marcus, P.; Światowska, J. Influence of Carbonate Solvents on Solid Electrolyte Interphase Composition over Si Electrodes Monitored by In Situ and Ex Situ Spectroscopies. *ACS Omega* **2021**, *6* (41), 27335−27350.
(37) McBrayer, J. D.; Harrison, K. L.; Allcorn, E.; Minteer, S. D. Chemical contributions to silicon anode calendar aging are dominant over mechanical contributions. *Front. Batteries Electrochem.* **2023**, *2*, No. 1308127.
(38) Stetson, C.; Yin, Y.; Jiang, C.-S.; DeCaluwe, S. C.; Al-Jassim, M.; Neale, N. R.; Ban, C.; Burrell, A. Temperature-Dependent Solubility of Solid Electrolyte Interphase on Silicon Electrodes. *ACS Energy Letters* **2019**, *4* (12), 2770−2775.

https://doi.org/10.1021/acsami.3c14361
ACS Appl. Mater. Interfaces 2024, 16, 19663−19671